# ChemComm

Accepted Manuscript


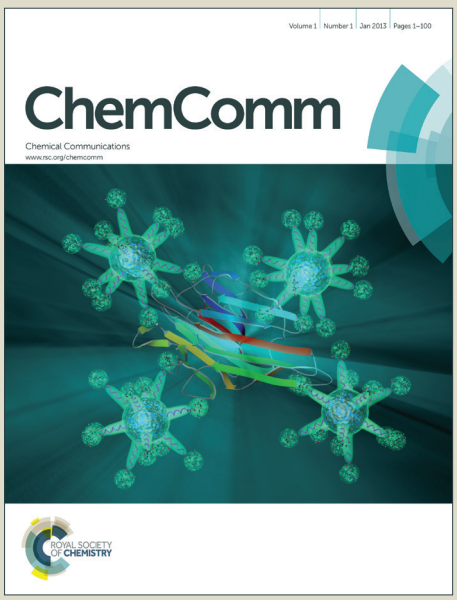





ROYAL SOCIETY OF CHEMISTRY

www.rsc.org/chemcomm

Journal Name

RSCPublishing

COMMUNICATION

# Thin films of spin-crossover coordination polymers with large thermal hysteresis loops prepared by nanoparticle spin coating

Cite this: DOI: 10.1039/x0xx00000x

Received 00th January 2012,
Accepted 00th January 2012

DOI: 10.1039/x0xx00000x

www.rsc.org/

Daisuke Tanaka,*[a] Naoki Aketa,[a] Hirofumi Tanaka,[a,b] Takashi Tamaki,[a] Tomoko Inose,[a] Tomoki Akai,[a] Hirotaka Toyama,[a] Osami Sakata,[c] Hiroo Tajiri,[d] and Takuji Ogawa*[a]

**This paper describes the synthesis of spin-crossover nanoparticles, which can disperse in various organic solvents without an excess amount of surfactant. The nanoparticles form homogeneous thin films on substrates by spin coating. The films show abrupt spin transition with large thermal hysteresis loops.**

Spin-crossover (SCO) phenomenon, which represents low-spin (LS) to high-spin (HS) transitions, have attracted wide attention because of their potential for sensor and memory applications.[1] In particular, some polymeric complexes, so called coordination polymers, show abrupt spin transition with large thermal hysteresis near room temperature caused by the strong cooperativity, and the bistability in the thermal hysteresis loop confers a memory effect.[2] To prepare memory and sensor devices based on SCO materials, versatile fabrication processes for polymeric SCO compounds are expected. The development of thin films and patterning of SCO compounds have recently been reviewed, and the processing of polymeric SCO complexes is often difficult because coordination polymers are generally insoluble and cannot be sublimated although unconventional lithographic processes for patterning and fabrication were successfully used to pattern spin-crossover compounds.[3] One technique for the processing of polymeric SCO complexes makes use of nanoparticles dispersed in matrixes that can form thin films and structures patterned by wet techniques, such as unconventional lithographic processes.[4] In particular, some nanoparticles with $[Fe(R\text{-}trz)_3]X_2$ formula (trz = triazole, X = anion) show abrupt spin transition with large hysteresis.[5] Coronado et al. have also shown that the spin transition temperature of $[Fe(Htrz)_{3-x}(NH_2trz)_x]$ type nanoparticles (Htrz = 1,2,4-4H-triazole, and $NH_2trz$ = 4-amino-1,2,4-triazole) decreases as the ratio of $NH_2trz$ increases, demonstrating that the SCO transition temperature can be controlled by changing the ratio of the ligands that were observed in bulk.[6] Making use of nanoparticles of the $[Fe(trz)_3]X_2$ family is most likely a promising strategy for patterning and device applications. The problem is, however, that the dispersion of the SCO nanoparticles with large thermal hysteresis loops has often required excess amounts of surfactant or matrixes, and thus, the films or patterned structures prepared with the nanoparticles included a large amount of the residual surfactant or matrixes. Herein, we have prepared nanoparticles of $[Fe(Htrz)_3]$ (**1**), $[Fe(Htrz)_{2.95}(NH_2trz)_{0.05}]$ (**2**), and $[Fe(Htrz)_{2.85}(NH_2trz)_{0.15}]$ (**3**) using anions of $ClO_4^-$; these nanoparticles can be dispersed in various solvents without using excess amounts of surfactant. The nanoparticles can form dense and homogeneous thin films by spin coating, and the films remain in abrupt spin transition behaviour with large thermal hysteresis.

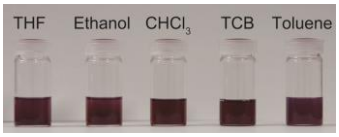


Fig. 1. The dispersion of **1** in various solvents.

The nanoparticles, **1**–**3**, were synthesized according to the method reported by Coronado et al.[6] They used the reverse micelle technique, in which the oil phase was *n*-octane, and the surfactant was behenic acid and AOT (dioctyl sulphosuccinate sodium salt). In their previous reports, the solid produced by slow evaporation of *n*-octane showed thermal hysteresis. The dried solid, however, included a large amount of surfactant ($Fe^{2+}$ : AOT = 1 : 10), and it was not removed. Then, we attempted to reduce the excess surfactant by washing with ethanol. The obtained purple nanoparticles after ethanol washing were collected by centrifugation. Interestingly, before drying in vacuo, the nanoparticles, wet with ethanol, can be well dispersed in various solvents, such as ethanol, THF, toluene, chloroform ($CHCl_3$), and 1,2,4-trichlorobenzen (TCB), providing a transparent solution, as shown in Fig. 1, although the previous report said that the nanoparticles with an excess amount of surfactant can be suspended again only in a nonpolar solvent.[5c, 6] Fig. S1 (ESI†) shows variable temperature UV-vis absorption spectra in heating and cooling modes for **1**–**3** dispersed in TCB. The absorption peak centred at 530 nm is assigned to the d-d transition of the LS state ($^1A_{1g}$ - $^1T_{1g}$), and the broad band at 800 nm is the d-d transition of the HS state ($^5T_{2g}$ - $^5E_g$). The absorption spectra demonstrated that the nanoparticles in TCB showed typical SCO transition. Temperature dependence of the absorbance at 530 nm for **1**–**3** in Fig. S2 (ESI†) indicates that the spin transition is clearly preserved with large thermal hysteresis. As expected, the thermal hysteresis moves to lower temperatures and becomes narrower as the ratio of $NH_2trz$ increases. The width of the hysteresis shown in Fig. S2 (ESI†) does not show a clear difference

between the first and second cycles, although the hysteresis of the previously reported solid in excess surfactant decreases after a few cycles. The detail is discussed in a later paragraph.

The purple precipitate collected by centrifugation after ethanol washing was dried in vacuo at room temperature, resulting in purple solid (Fig S3, ESI†). After the drying process, the solid cannot be dispersed again in any solvent, and this feature of the nanoparticles would be suitable for printable fabrication applications because, after processing, the dried nanoparticle becomes stable to solvent extraction. Magnetic measurements were performed on the dried nanoparticles of **1**–**3** by a superconducting quantum interference device (SQUID). As shown in Fig. 2, Fig S4, and Fig S5 (ESI†), the spin transition is preserved in the solid state. The $\chi_M T$ versus $T$ curves reveal abrupt transitions occurring with large hysteresis loops. The magnetic curves indicate that the thermal hysteresis shifts to lower temperature and becomes narrower as the ratio of 4-$NH_2$trz increases. Furthermore, in the second heating and cooling cycle, the hysteresis loop becomes narrower than that of the first heating cycle. This tendency is consistent with the previous reports. The spin transition temperature estimated from differential scanning calorimetry (DSC) measurements for the dried nanoparticles of **1**–**3** has also shown the same tendency (Fig. S6, ESI†). Considering the enthalpy variations ($\Delta H$) in the first heating mode as typical examples, the values of $\Delta H$ for **1**, **2,** and **3** are estimated as 24.4, 20.8, and 15.2 kJ $mol^{-1}$, respectively. The absolute value of $\Delta H$ is consistent with previously reported values for $[Fe(R\text{-}trz)_3]X_2$ type complexes.[7] Doping 4-$NH_2$trz ligand results in a reduction of $\Delta H$ and, hence, in the lowering of the critical temperatures.[8]

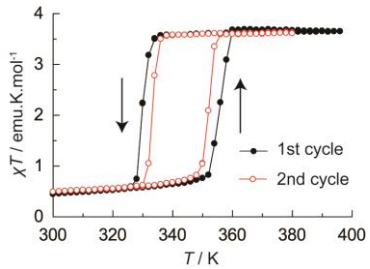


Fig. 2. Magnetic thermal hysteresis for the dried nanoparticles of **1** under 1000 Oe.

The values of spin transition temperatures estimated from absorption spectrum, magnetic measurement, and DSC measurement are summarized in Fig. 3, Fig. S7, and Fig. S8 (ESI†). Herein, the temperatures of $T_c\uparrow$ and $T_c\downarrow$ for magnetic measurement and UV-vis absorption spectrum are defined as the temperatures at which 50% of both the LS and the HS molecules are in the heating and cooling modes, respectively. The transition temperatures for DSC are the peak top in heating and cooling mode. The bar charts in Fig. 3 demonstrate that the transition temperatures of **1** in the first heating cycle shows clear dependency on the measurement methods. The $T_c\uparrow$ estimated from the UV-vis absorption spectrum is lower and the hysteresis is smaller than the others. In the second cycle, however, $T_c\uparrow$ estimated from magnetic measurements and DSC measurements are shifted to a lower temperature, whereas $T_c\uparrow$ and $T_c\downarrow$ from the absorption spectrum does not change. The obtained transition temperatures in second cycle show smaller differences between the measurement methods. The same tendency was observed in **2** and **3**. The absorption spectrum was measured in TCB, although magnetic measurements and DSC were carried out in the dried nanoparticles. Therefore, the specificity of $T_c\uparrow$ estimated from the absorption spectrum would be attributed to the existence of TCB. The transition behaviour of the $[Fe(Htrz)_3](ClO_4)_2$ family in the bulk form is drastically changed by the adsorption of non-coordinated water.[8] Thus, one hypothesis is that water molecules in the crystal lattice of the nanoparticles might be released from the nanoparticles in TCB before heating, whereas the water in the dried nanoparticle remains before the heating cycle, and the water desorption occurs in the first heating cycle. However, thermogravimetric analysis of **1**–**3** in the dried nanoparticles demonstrated that no weight loss was observed below 400 K, indicating that water desorption does not occur or is very limited, and, thus, the difference between measurement methods cannot be explained by the simple water desorption. On the other hand, the magnetic measurements have revealed that the high relative magnetic moment found at low temperatures, which would originate from surface defects, and the residual HS component at low temperature increase after a heating cycle (Fig. 2, Fig. S4, and Fig. S5, ESI†).[5c] The outcome suggests that the heating cycle induces some reorganization in the dried-nanoparticle surface, resulting in the increasing of the defect that has the HS component. A recent report revealed that matrices surrounding SCO nanoparticles have a dramatic effect on the cooperative spin-crossover phenomenon, indicating that the surface environment of SCO nanoparticles is one of the dominant parameters for phase transition.[9] We would suppose that the differences between the first and second cycles can be attributed to the surface reorganization in the dried nanoparticles, and the reorganization might be prevented in TCB or finished before heating. In the previous report, the thermal hysteresis loops of the nanoparticles after several heating and cooling processes become stable loop. The dried nanoparticles in this report would also show stable hysteresis width after further heating and cooling cycles.

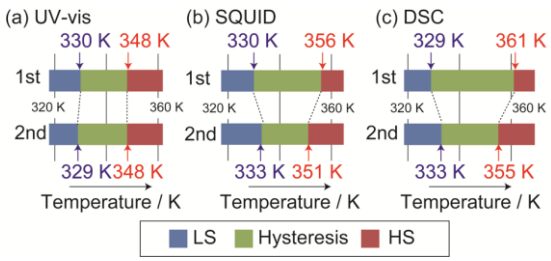


Fig. 3. The summary of $T_c\uparrow$ and $T_c\downarrow$ for **1** estimated from UV-vis absorption spectrum (a), magnetic measurement (b), and thermal analysis (c). The red and blue characters represent $T_c\uparrow$ and $T_c\downarrow$, respectively.

We have demonstrated that the nanoparticles prepared here can be dispersed in various solvents and remain in abrupt SCO behaviour. These properties are suitable for wet process patterning. As a demonstration, thin films of **1**–**3** were prepared on substrates. Surface coating was carried out by spin coating an ethanol solution of **1**–**3**. Field-emission scanning electron microscopy (FE-SEM) pictures showed that the nanoparticles form homogeneous densely packed thin films on silicon surfaces (Fig. 4a and Fig. S9, ESI†). A high-magnification image of FE-SEM, however, cannot be obtained because charge-up occurs and the samples are damaged. To estimate the precise structures, the films were observed by atomic force microscopy (AFM). Fig. 4b, Fig S10 and Fig. S11 in ESI† show that the nanoparticles on the $SiO_2$ surfaces were observed as homogeneous thin films. The height or thickness of the steps on thin films is approximately 18 nm, as shown in Fig. 4c and the roughness parameter, $R_a$, is 19.5 nm, which is consistent with the previously reported particle size of **1**. An AFM image with high magnification in ESI (Fig. S11) shows that the particles strongly aggregate on the surface and the particle size is approximately 20 nm. These results have demonstrated that the coalescence of particles and the formation of objects with larger sizes was not observed and that the SCO coordination polymers retain their original particle morphology. The particles can be printed on surfaces densely by simple wet processes

such as spin coating and ink-jet printing. The thin film of SCO coordination polymers prompted us to explore their SCO transition behaviour. The amount of the sample on the substrate, however, is tiny, and the detection of the phase transition signal is difficult. To monitor the SCO behaviour of the tiny amount of compounds on the substrates, synchrotron X-ray diffraction (XRD) measurements were carried out in in-plane mode under various temperatures. Fig. 4d and 4e show the XRD pattern for **1** on $SiO_2$ in the first heating and cooling cycle. The diffraction pattern clearly showed that the crystal structure transition occurred at a particular temperature. In the heating mode, all peaks shift to a lower angle at 353 K, indicating lattice expansion or the transition to the HS state. During the following temperature ramp-down, the film of **1** stayed at the HS state, and at 333 K, the structure changes back to the LS state. The XRD peak position after a heating cycle reverted to the original patterns, suggesting that no crystal lattice deformation caused by water desorption occurs during the heating and cooling cycle. Figs. S12–S17 in ESI† show the temperature dependency of XRD patterns of **1**–**3** in the first and second heating cycles. These results clearly demonstrate that the thin films on $SiO_2$ remain in their SCO transition property.

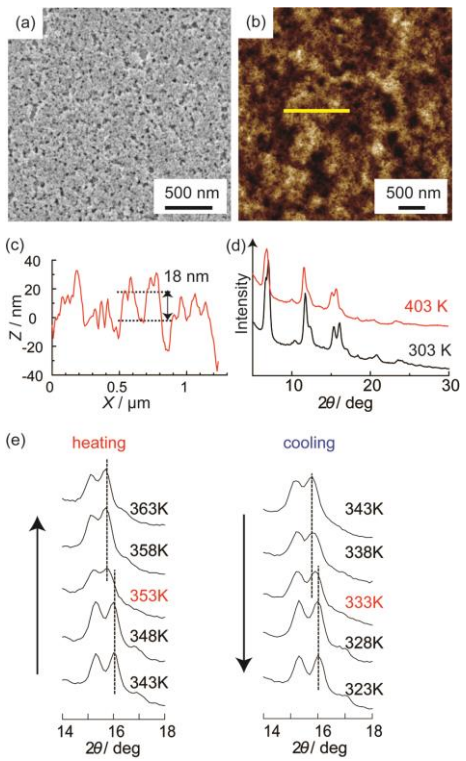


Fig. 4. (a) FE-SEM image and (b) topographic AFM image of the thin film of **1**. (c) Cross section of the yellow line in (b). (d) The synchrotron XRD patterns of **1** in in-plane mode on $SiO_2$ substrates in LS (black) and HS (red) during the first heating. (d) The XRD patterns of thin film **1** in the first heating and cooling mode.

The reported SCO transition temperatures of bulk $[Fe(Htrz)_{3-x}(NH_2trz)_x](ClO_4)_2$ are approximately 30 K lower than those of **1**-**3**.[8] Generally, SCO nanoparticles possess a lower transition temperature than that of bulk due to the loss in cooperativity; however, we observed an opposite trend in this study. Furthermore, the XRD patterns of the thin films of **1**-**3** were clearly different from the patterns of bulk samples prepared using a previously reported method (Fig. S18, ESI†).[8] The comparison of nanoparticles with bulk samples strongly suggests that the crystal structures of the nanoparticles are not the same as those of bulk samples. In contrast, XRD patterns of $[Fe(trz)(Htrz)_2](BF_4)$ are quite similar to those of **1**-**3** (Fig. S18, ESI†).[10] It is known that bulk $[Fe(trz)(Htrz)_2](BF_4)$ shows a higher SCO temperature than $[Fe(Htrz)_{3-x}(NH_2trz)_x](ClO_4)_2$,[7] which is consistent with the high transition temperatures of **1**-**3**. Because the size of $BF_4^-$ is similar to that of $ClO_4^-$ and because there is no solvent accessible space in the crystal lattice of $[Fe(trz)(Htrz)_2](BF_4)$, **1**-**3** are most likely to include only one $ClO_4^-$ anion per $Fe^{2+}$ ion in their crystal lattice. Results of the elemental analysis (EA) of **1**-**3** are in good agreement with that expected from the chemical composition of $[Fe(trz)(Htrz)_{2-x}(NH_2trz)_x](ClO_4)_{1.2}(AOT)_{0.08}$. The values plotted on the y-axis in Fig. 2 and Fig. S7-8 in ESI† were calculated using the above chemical formula. The $\chi_M T$ values obtained at high temperatures are agree well with those previously reported for bulk samples, 3 to 3.5 $cm^3\ mol^{-1}\ K$.[5a] This suggests that the values expected from the formula are similar to the actual values. The excess of 0.2 molecules of $ClO_4^-$ per Fe ion might be attributed to the presence of surface defects or inorganic impurity. By assuming that (1) 0.08 molecules of AOT remain on the surface, (2) the particle is a sphere with a diameter of 20 nm, and (3) the unit cell of the nanoparticle is the same as that of $[Fe(Htrz)_2(trz)](BF_4)$, we could demonstrate using a simple geometric calculation that the AOT molecules would exist on the surface at an interval of about 1.4 nm. The small amount of residual surfactant on the surface would explain the stability of the sample dispersion after washing and strong aggregation after complete drying; the low coverage of surfactant could not prevent strong adhesion after removal of the solvents from the surface.

In summary, the nanoparticles of the $[Fe(trz)_3]$ type SCO coordination polymers, **1**–**3**, were synthesized. We have demonstrated that the nanoparticles prepared here remain in abrupt SCO behaviour confirmed by UV-vis absorption spectrum, magnetic measurements, and DSC, and the residual surfactant is small. The nanoparticles can be dispersed in various solvents and can form homogeneous thin film on substrates by spin coating. The AFM measurement reveals that the nanoparticles are strongly aggregated and deposited on the surfaces, resulting in thin films. Synchrotron XRD in in-plane mode demonstrates that the SCO transition occurs even in the thin films. These results prove that the suspension of **1**–**3** would be suitable for device fabrication of SCO coordination polymers by printed electronics techniques, such as ink-jet printing and soft lithography, although further optimization of the solution property for wet lithography are required.[11] Furthermore, one of the advantages of our method is that composite film can be easily prepared and the property of the thin films can be controlled easily. A study of the electrical properties of the devices prepared with the thin films is currently in progress.

This study was supported in part by Grants-in-Aid for Scientific Research (No. 23310076, 23750162, 24651142, 25706005) and for Scientific Research on Innovative Areas from the Ministry of Education, Culture, Science, Sports, and Technology of Japan No. 25110002 (Molecular Architectonics: Orchestration of Single Molecules for Novel Functions)). This work is partially supported by Kurata Grants from The Kurata Memorial Hitachi Science and Technology Foundation, Ogasawara Foundation and the Kao Foundation for Arts and Sciences. The synchrotron radiation experiments were performed at the BL13XU of SPring-8 with the approval of the Japan Synchrotron Radiation Research Institute (JASRI) (Proposal No. 2011A1462, 2011B1495, and 2012A1204).

## Notes and references

[a] Department of Chemistry, Graduate School of Science, Osaka University, 1-1 Machikaneyama, Toyonaka, Osaka 560-0043, Japan

[b] Present address:Department of Human Intelligence Systems, Graduate School of Life Science and Systems Engineering, Kyushu Institute of Technology, Kitakyushu, Japan.

[c] Synchrotron X-ray Station at SPring-8, National Institute for Materials Science, Sayo-gun, Hyogo, Japan.
[d] Japan Synchrotron Radiation Research Institute/SPring-8, Sayo-gun, Hyogo, Japan.

†Electronic Supplementary Information (ESI) available: details of the experiment, UV-vis absorption spectrum, magnetic hysteresis, DSC, summary of the phase transition temperature and XRD patterns. See DOI: 10.1039/c000000x/

1. P. Guetlich and H. A. Goodwin, *Topics in Current Chemistry, Vols. 233, 234 and 235*, Springer, Berlin, Heidelberg, New York,, 2004.
2. (a) O. Kahn and C. J. Martinez, *Science*, 1998, **279**, 44; (b) J. A. Real, A. B. Gaspar, V. Niel and M. C. Munoz, *Coordin. Chem. Rev.*, 2003, **236**, 121; (c) P. Gutlich, Y. Garcia and T. Woike, *Coordin. Chem. Rev.*, 2001, **219**, 839; (d) G. a. Moln´ar, L. Salmon, W. Nicolazzi, F. Terki and A. Bousseksou, *J. Mater. Chem. C*, 2014, **2**, 1360.
3. (a) M. Cavallini, *Phys. Chem. Chem. Phys.*, 2012, **14**, 11867; (b) M. Cavallini, I. Bergenti, S. Milita, G. Ruani, I. Salitros, Z. R. Qu, R. Chandrasekar and M. Ruben, *Angew Chem Int Edit*, 2008, **47**, 8596; (c) M. Cavallini, I. Bergenti, S. Milita, J. C. Kengne, D. Gentili, G. Ruani, I. Salitros, V. Meded and M. Ruben, *Langmuir*, 2011, **27**, 4076.
4. C. Thibault, G. Molnar, L. Salmon, A. Bousseksou and C. Vieu, *Langmuir*, 2010, **26**, 1557.
5. (a) O. Roubeau, *Chem-Eur J.*, 2012, **18**, 15230; (b) H. J. Shepherd, G. Molnar, W. Nicolazzi, L. Salmon and A. Bousseksou, *Eur J Inorg Chem*, 2013, **2013**, 653; (c) E. Coronado, J. R. Galan-Mascaros, M. Monrabal-Capilla, J. Garcia-Martinez and P. Pardo-Ibanez, *Adv. Mater.*, 2007, **19**, 1359; (d) T. Forestier, A. Kaiba, S. Pechev, D. Denux, P. Guionneau, C. Etrillard, N. Daro, E. Freysz and J. F. Letard, *Chem-Eur J.*, 2009, **15**, 6122; (e) A. Tokarev, L. Salmon, Y. Guari, W. Nicolazzi, G. Molnar and A. Bousseksou, *Chem. Commun.*, 2010, **46**, 8011; (f) F. Prins, M. Monrabal-Capilla, E. A. Osorio, E. Coronado and H. S. J. van der Zant, *Adv. Mater.*, 2011, **23**, 1545; (g) K. Kuroiwa and N. Kimizuka, *Polym J*, 2013, **45**, 384.
6. J. R. Galan-Mascaros, E. Coronado, A. Forment-Aliaga, M. Monrabal-Capilla, E. Pinilla-Cienfuegos and M. Ceolin, *Inorg. Chem.*, 2010, **49**, 5706.
7. J. Krober, J. P. Audiere, R. Claude, E. Codjovi, O. Kahn, J. G. Haasnoot, F. Groliere, C. Jay, A. Bousseksou, J. Linares, F. Varret and A. Gonthiervassal, *Chem. Mater.*, 1994, **6**, 1404.
8. J. Krober, E. Codjovi, O. Kahn, F. Groliere and C. Jay, *J. Am. Chem. Soc.*, 1993, **115**, 9810.
9. Y. Raza, F. Volatron, S. Moldovan, O. Ersen, V. Huc, C. Martini, F. Brisset, A. Gloter, O. Stephan, A. Bousseksou, L. Catala and T. Mallah, *Chem. Commun.*, 2011, **47**, 11501.
10. A. Urakawa, W. Van Beek, M. Monrabal-Capilla, J. R. Galan-Mascaros, L. Palin and M. Milanesio, *J Phys Chem C*, 2011, **115**, 1323.
11. (a) D. Qin, Y. N. Xia and G. M. Whitesides, *Nat Protoc*, 2010, **5**, 491; (b) M. Cavallini, D. Gentili, P. Greco, F. Valle and F. Biscarini, *Nat Protoc*, 2012, **7**, 1668.



 